International Journal of Thermal Sciences 49 (2010) 829–837

Contents lists available at ScienceDirect

International Journal of Thermal Sciences

journal homepage: www.elsevier.com/locate/ijts

Forced convection of the brass-beads packed bed situated in a vertical oncoming flow

Tzer-Ming Jeng [a,*], Sheng-Chung Tzeng [b], Chia-Wei Chang [b]

[a] Department of Mechanical Engineering, Air Force Institute of Technology, GangShan 820, Taiwan, ROC
[b] Department of Mechanical Engineering, Chienkuo Technology University, ChanGhua 500, Taiwan, ROC

ARTICLE INFO

Article history:
Received 6 January 2009
Received in revised form
14 September 2009
Accepted 9 November 2009
Available online 26 November 2009

Keywords:
Heat transfer
Pressure drop
Brass-beads packed bed

ABSTRACT

This study experimentally investigated the convective heat transfer and pressure drop of a vertical oncoming airflow onto the brass-beads packed bed. The 120 mm-length (L) brass-beads packed bed was fully filled in a horizontal rectangular channel having a cross section of 60 mm width (W) and variable height (H). The flow entry, with variable width (w_j), was located at the center of the upper wall of the test channel. Besides, three kinds of packed beds with various bead diameters (d) were used herein. The ranges of relevant parameters were $w_j/L = 0.212-1$, $H/L = 0.083-0.25$ and $d = 2-6$ mm. Experimental results reveal that, at $w_j/L = 0.212$, the local Nusselt number (Nu) at the stagnation point ($x/L = 0$) right under the flow entry was maximal and then monotonically decreased along the transverse flow direction. However, when $w_j/L = 0.583$ and 1, the Nu firstly decreased from $x/L = 0$ to $x/L = 0.1$, then rose along the transverse flow direction. Additionally, under the same pumping power, the largest average Nusselt number ($\overline{Nu}$) appeared on $w_j/L = 0.212$, $H/L = 0.083$ and $d = 6$ mm, and the smallest $\overline{Nu}$ happened at $w_j/L = 1$, $H/L = 0.25$ and $d = 2$ mm. The largest $\overline{Nu}$ was around 3 times of the smallest $\overline{Nu}$. This work systemically completed the parametric studies on heat transfer and pressure drop. The relevant correlations of experimental results were also presented.

1. Introduction

While electronic components becomes more and more compact and multi-functional, the heat generation of unit volume will continuously increase, thus exerting immediate impact on their working efficiency, operational stability and service life. Therefore, how to remove efficiently the heat from electronic components is an important project in the industry and academia. Installing heat sink was already proved to be a cost-effective cooling technology, especially for the porous medium heat sink that has a bigger heat exchange area than traditional finned heat sink [1–8]. However, many researches were only devoted to heat transfer behavior of porous medium heat sink situated in the transverse flow channel. The impinging jet cooling was demonstrated having the capability of enhancing local heat transfer [9,10], so its combination with porous medium heat sink may yield higher cooling efficiency.

It is found from literature review that most of heat transfer studies about porous medium heat sink with impinging jet were based on numerical calculations. For example, Fu and Huang [11,12] numerically investigated the cooling performance of different porous blocks under free slot impinging jet, and employed porous empirical equation of spherical packed beds for resolving momentum equation; meanwhile, a single-equation model was employed to build energy equation by assuming that the fluid and porous medium are in the local thermal equilibrium state, pointing out that the amount of fluids near the heated surface strongly influences overall heat transfer performance. The other influential factors include the ratio of tip clearance to nozzle width, the ratio of porous block height to nozzle width, the shape of porous blocks, categories of porous materials and fluid flows, the velocity profile at exit of jet nozzle and the jet Reynolds number. In addition, Jeng and Tzeng [13] numerically discussed the heat transfer characteristics of Al-foam under a confined slot impinging jet, finding that the heat transfer capability improves with the lowering height of Al-foam, and the local thermal non-equilibrium exists between fluid and solid. In other words, it should build up energy equation by using the two-equation model. The jet-nozzle width, in the study of Jeng and Tzeng [13], was much smaller than the length of Al-foam. Although many numerical researches had considered the heat transfer performance of porous medium heat sink under impinging jet [14–19], few experimental studies have addressed this issue. Kim et al. [20] investigated experimentally the effects of the pore density of Al-foam, the jet velocity, the jet-to-jet spacing and the nozzle plate-to-heated surface separation distance in a 3 × 3 square

* Corresponding author. Tel.: +886 7 6256040; fax: +886 4 7357193.
E-mail addresses: tm.jeng@msa.hinet.net, t_m_jeng@yahoo.com.tw (T.-M. Jeng).

1290-0729/$ – see front matter © 2009 Elsevier Masson SAS. All rights reserved.
doi:10.1016/j.ijthermalsci.2009.11.006

multi-jet impinging array on the average Nusselt number. The used Al-foam heat sinks in above work were 100 mm in length, 90 mm in width and 10 mm in height. The jet-nozzle diameters were 12 mm and 4 mm for the single-jet mode and the multi-jet mode, respectively. Kim et al. [20] indicated that the Nusselt number of 10 PPI Al-foam heat sink was higher than that of 20 or 40 PPI Al-foam heat sink. Besides, under the condition of high jet Reynolds number and smaller jet-to-jet spacing, the multi-jet impingement showed higher heat transfer performance than the single-jet impingement. Shih et al. [21] studied experimentally the effect of the Al-foam height on the heat transfer of an Al-foam cylinder subject to the circular impinging jet. Their Al-foam cylinders were 65 mm in diameter and the jet-nozzle diameter was also 65 mm. Shih et al. [21] reported that the average Nusselt number first increased and then decreased with reducing the Al-foam height. In addition, decreasing the porosity and pore density increased the average Nusselt number. Jeng and Tzeng [22,23] discussed experimentally the heat transfer characteristics of Al-foam under the 90-deg turned flow and confined slot impinging jet, finding that the pore density of Al-foam and the jet-nozzle width have little influence on heat transfer, but the reduction of the jet-to-foam tip distance slightly improve heat transfer. However, the jet-nozzle width in Jeng and Tzeng [22,23] was much smaller than the length of Al-foam.

This work experimentally investigated the fluid flow and heat transfer characteristics of the vertical oncoming airflow onto the brass-beads packed bed. The brass-beads packed bed, sized by 120 mm in length (L), 60 mm in width (W) and variable height (H) with porosity about 0.38–0.47, was fully filled in a rectangular horizontal channel. The permeability of the brass-beads packed bed drops significantly as compared with high-porosity Al-foam whose porosity is over 0.9, so the forced convective heat transfer behaviors in such tow porous blocks should be very different. This work designed the flow entry, located at the center of the upper wall of the test channel, was rectangular cross section with variable width (w_j). Variable parameters were the Reynolds number (Re), the ratio of entry width to Al-foam length (w_j/L), the ratio of Al-foam height to length (H/L) and the bead diameter (d), of which the value of w_j/L reached 1. The objectives were to understand the effects of relevant parameters on local and average heat transfer, pressure drop and propose the optimal parameter mode of maximum heat transfer capability generated under the given pumping power for further reference.

2. Experimental setup

2.1. Test section and apparatus

The experimental system, as shown in Fig. 1, includes: (a) air supply system, (b) test section, (c) heating and temperature measurement system, and (d) data acquisition system.

(a) Air supply system: The wind tunnel was made of 10 mm-thick Plexiglas plates. The main flow of air was supplied by a blower, and the flow rate was controlled by using an inverter to regulate the AC frequency of the blower's motor (0.5 Hp). Prior to entering into the test section, air would pass through a straightening section and a convergent section. The straightening section was made of spherical packed bed and multi-layer fine-mesh stainless steel screens. Three kinds of convergent sections, respectively with the exits of 25.4 mm × 60 mm, 70 mm × 60 mm and 120 mm × 60 mm cross-sections, were employed to change the flow entry width (w_j). Finally, air blew down into the test section vertically.

(b) Test section: The test section, made of 20 mm-thick Plexiglas plates, was a horizontally rectangular channel with 600 mm in length, 60 mm (W) in width and variable heights (H = 10, 20 and 30 mm). The flow entry was coupled at the center of the upper wall of the test channel. The 120 mm-length (L) brass-beads packed bed was fully filled into the test channel rightly under the flow entry. The brass beads were available with the diameter (d) of 2 mm, 4 mm and 6 mm. The average porosities (ε) of the brass-beads packed beds were measured and listed in Table 1. As the photo in Fig. 2, the brass-beads packed bed was confined and fixed by the fine-mesh stainless steel screen, and was positioned on a heating system. Table 1 indicates that the porosity (ε) increased with bead diameter (d), but decreased as increasing height (H) of packed bed. Achenbach [24] reviewed the heat and flow characteristics of packed beds and reported that, the porosity decreases from unity at the wall to a constant value. This point is reached at a distance of around two to four bead diameters from the wall. The constant value of porosity at the core region of packed bed is around 0.37. This is the so-called theory of the variable porosity. The average porosity (ε) will be the volume weighted mean value of the core-region porosity (ε_∞) and the near-wall-region porosity (ε_{nw}). When the volume ratio of packed bed to bead is bigger, the average porosity (ε) is more near the core-region porosity (ε_∞). The measured results in Table 1 conformed to the above-mentioned statement.

(c) Heating and temperature measurement system: The system body, sized by 170 mm in length, 78 mm in width and 60 mm in height, was made of Bakelite. The thermal conductivity of Bakelite was only 1.4 W/m/K, presenting excellent heat insulation. On the upper surface of the Bakelite body, 7 long grooves (shown in Fig. 2) were notched, each of which was embedded with a long copper bar of 60 mm × 4.5 mm × 4.5 mm. The heads of thermocouples (OMEGA TT-T-30-SLE) were welded

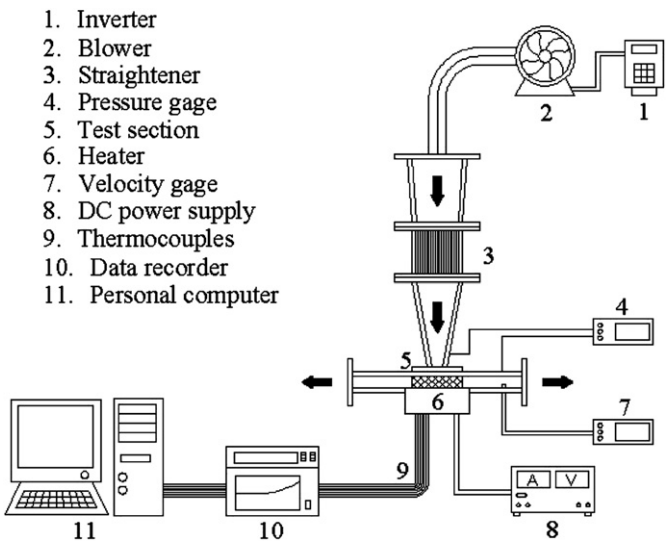

Fig. 1. Experimental setup.

Table 1
Measured porosities of the brass-beads packed beds (64.2%Cu + 35.8%Zn).

Measured porosity (ε) (stagnant conductivity, W/m/K)	d = 2 mm	d = 4 mm	d = 6 mm
H = 30 mm	0.383 (0.578)	0.399 (0.538)	0.412 (0.508)
H = 20 mm	0.391 (0.558)	0.410 (0.512)	0.428 (0.473)
H = 10 mm	0.404 (0.526)	0.436 (0.456)	0.467 (0.398)

The stagnant conductivity of the brass-beads packed bed was estimated by the formula in Refs. [11,12]. The conductivities of brass and air are about 116 and 0.027 W/m/K, respectively.

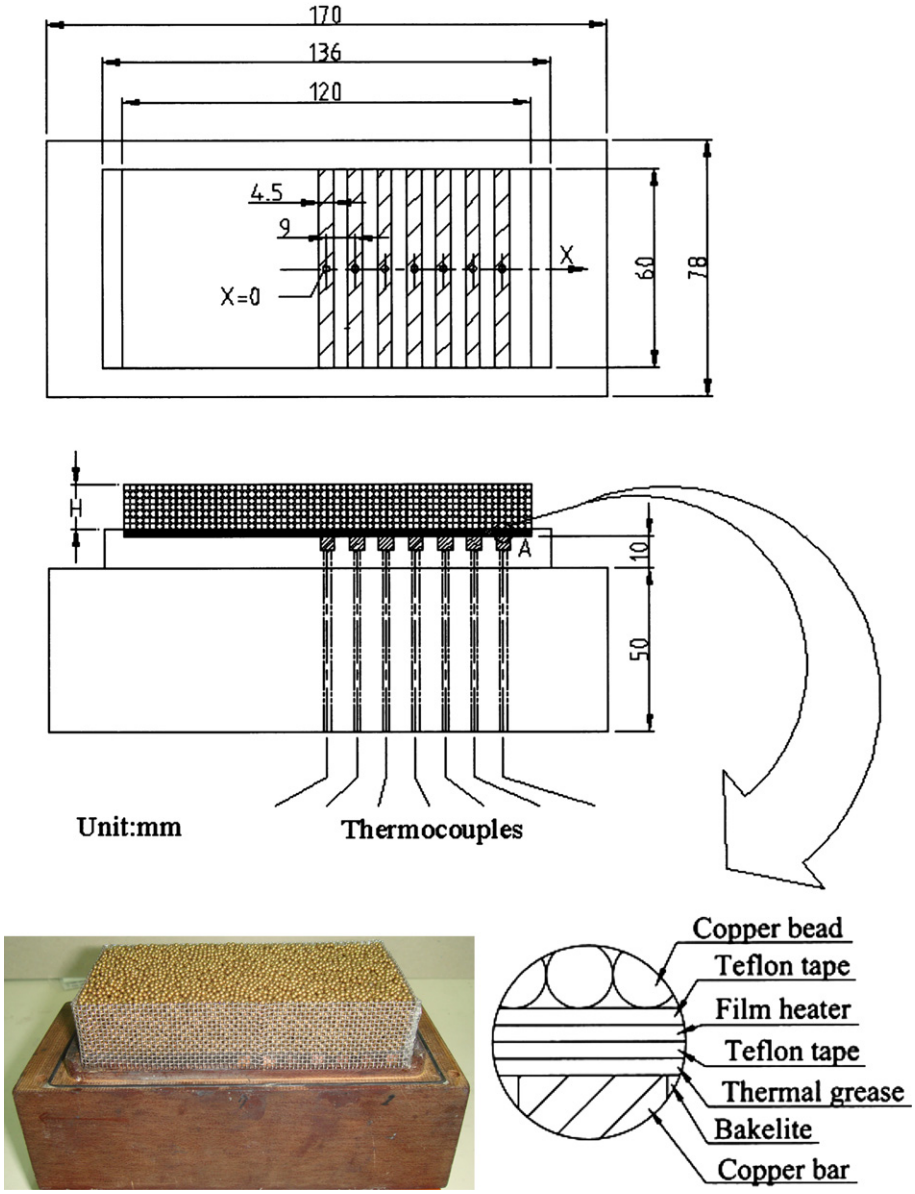

Fig. 2. Photo of brass-beads packed bed and positions of thermocouples (the upper surface of packed bed was confined by the stainless screen in performing tests).

onto the copper bars. The thermocouple wires passed through the Bakelite body, and then were connected to the data recorder. A stainless steel film heater of 120 mm × 60 mm was attached on the upper surface of the copper bars by using the high-conductivity thermal grease. Both sides of the film heater were adhered with Teflon tapes to prevent direct contact with brass-beads and copper bars. In addition to heated wall temperatures (T_w), air temperature at flow entry (T_j) and the ambient temperatures (T_∞) were also measured.

(d) Data acquisition system: This system comprised a data recorder (YOKOGAWA DA-100), an anemometer (KANOMAX Model 6112) and a pressure transmitter (DWYER Model 648-4). The data recorder was used to record temperatures sensed by thermocouples. The steady temperature was judged based on that the temperature change was less than 0.2 °C within 15 min. The average air velocity at flow entry (V_j) was converted from the average air velocity at transverse exit (U_e) of the test channel ($V_j = 2U_e \times H/w_j$). The U_e was measured by the anemometer at 100 mm away from brass-beads packed bed.

The static pressure difference (ΔP) of air flowing through brass-beads packed bed is measured by the pressure transmitter.

2.2. Data reduction and uncertainty analysis

The average air velocity (V_j) at flow entry, static pressure difference (ΔP), various temperatures (T_w, T_∞, T_j) can be used to determine the relevant dimensionless parameters, such as Reynolds number (Re), friction coefficient (C_f) and Nusselt number (Nu), are defined below.

$$Re = \frac{\rho_f V_j w_j}{\mu} \tag{1}$$

$$C_f = \frac{\Delta P + 0.5\rho_f\left(V_j^2 - U_e^2\right)}{0.5\rho_f V_j^2} \tag{2}$$

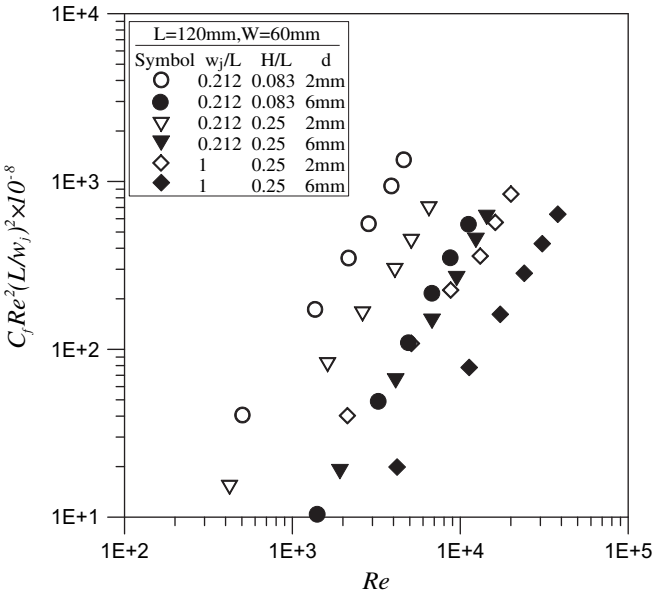

Fig. 3. Dimensionless pressure drop as a function of Re for various w_j/L, H/L and d.

$$Nu = \frac{hL}{k_f} = \frac{(Q_{in} - Q_{loss})L}{A(T_w - T_j)k_f} \tag{3}$$

$$\overline{Nu} = \sum_{i=1}^{7} Nu_i \cdot \Delta S_i/(0.5L) \tag{4}$$

Where V_j is the average air velocity at flow entry, U_e is the average air velocity at transverse exit of the test channel, w_j is the flow entry width, T_w is the heated wall temperature, T_j is the air temperature at flow entry, ΔP is the static pressure difference, L is the length of brass-beads packed bed, Q_{in} is the input heat, Q_{loss} is the heat loss, A is the heated area, and ΔS is the spacing between adjacent thermocouples.

To estimate the heat loss, the flow entry and both exits of the empty channel are fully sealed by Polystyrene blocks. Therefore, when the heated wall temperatures reach steady–state condition, the input heat from the film heater equals to the heat loss dissipated from the Bakelite body to the ambient.

$$Q_{in} = V \times I = Q_{loss} = h_{loss}A(T_w - T_\infty) \tag{5}$$

During estimation of heat loss, various quantities of heat are separately input to the film heater, while the heated wall

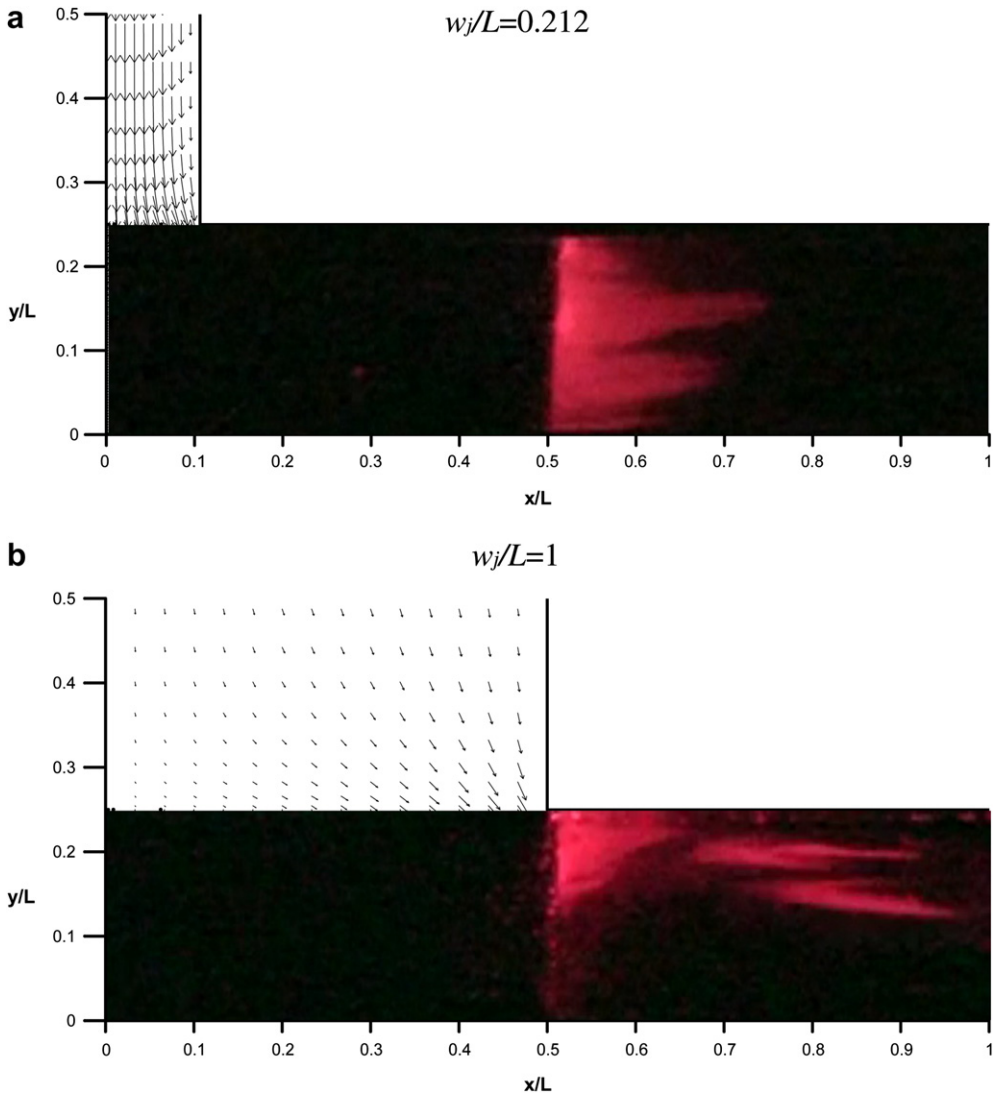

Fig. 4. Flow visualizations in the typical cases of $H/L = 0.25$, $d = 4$ mm and $Re = 858$ with various values of w_j/L.

temperature (T_w) and ambient temperature (T_∞) are recorded when the temperatures reach steady-state condition; the empirical formula of heat loss is found out using the relationship of T_w, T_∞ and input heat (Q_{in}).

The overall error of experimental results includes the uncertainties of measurement and calculation, of which the uncertainty of measurement is caused from the error of the instrument and manual reading, and the calculation uncertainty is obtained from alternative computations of measured data. Herein, data supplied by the manufacturer of the instrumentation states that the measurement of flow velocity and pressure drop have a 1% error. The uncertainty in the measured temperature is ±0.2 °C. The experimental uncertainty in the heat loss (Q_{loss}) is estimated to be 3.6%. With the standard single-sample uncertainty analysis recommended by Kline and Mcclintock [25] and Moffat [26], it reveals that the uncertainties in Reynolds number (Re), friction coefficient (C_f), local Nusselt number (Nu) and average Nusselt number ($\overline{Nu}$) are ±2.45, ±3.46, ±6.32, ±7.11, respectively.

3. Results and discussion

3.1. Pressure drop

Fig. 3 depicts the relationship between dimensionless pressure drop ($C_f Re^2 (L/w_j)^2$) and Reynolds number (Re) for various w_j/L, d and H/L. The results show that dimensionless pressure drop increased with Re. The pressure drop of fluid flow through porous medium is primarily caused by two factors: 1. the skin friction, which is proportional to the fluid rate; 2. the form drag generated from the collision, separation and combination of fluid flowing through porous structure, which is proportional to the double power of the fluid rate. The experimental results indicate that, within the most ranges of parameters herein, the pressure drop from form drag had a similar magnitude with that from skin friction. As indicated in Fig. 3, when the w_j/L was equal to 1, most airflow should from the upper corners of the porous packed bed to leave due to the minimum flow resistance of these paths, leading to reduction of overall pressure drop. In the cases of $w_j/L = 0.212$, their pressure drops were smaller than those of $w_j/L = 1$ since airflow had no chance to leave rapidly the packed bed. Besides, the cases of smaller bead diameter had bigger pressure drops owing to the fact that it has a bigger total extended area and higher pore density within the smaller bead diameter packed bed. Furthermore, the case of smaller H/L generally had a bigger pressure drop because that the smaller H/L results in a bigger transverse fluid velocity. However, the effect of H/L on pressure drop was insignificant in the case of big bead diameter (e.g. $d = 6$ mm). As we know, although small H/L results in big transverse fluid velocity to increase pressure drop, it also decreases the total bead numbers to reduce the skin friction. Especially, in the case of small H/L with big bead diameter

Table 2
Coefficients of Eq. (6): $C_f Re^2 (L/w_j)^2 = m_1 Re^{n_1}$.

w_j/L	H/L	Re	m_1	n_1
$d = 2$ mm				
0.212	0.083	504–4603	187 842	1.588
0.212	0.167	733–6824	68 066	1.538
0.212	0.250	422–6503	311 482	1.389
0.583	0.083	648–6033	46 847	1.704
0.583	0.167	982–8149	205 879	1.471
0.583	0.250	1489–11 699	94 419	1.507
1	0.083	1668–13 622	23 815	1.620
1	0.167	2169–17 967	68 079	1.433
1	0.250	2123–20 035	134 883	1.332
$d = 4$ mm				
0.212	0.083	863–5878	237	2.224
0.212	0.167	1099–11 130	61 617	1.465
0.212	0.250	1534–11 887	7213	1.701
0.583	0.083	1112–7916	2973	1.967
0.583	0.167	1361–12 831	161 592	1.426
0.583	0.250	2105–14 829	20 808	1.613
1	0.083	2194–15 134	375	2.024
1	0.167	1632–25 832	232 845	1.248
1	0.250	3059–31 301	22 155	1.436
$d = 6$ mm				
0.212	0.083	1413–11 278	369	2.030
0.212	0.167	1541–13 383	13 065	1.601
0.212	0.250	1919–14 380	4889	1.704
0.583	0.083	1585–11 880	3594	1.844
0.583	0.167	2248–17 963	30 154	1.544
0.583	0.250	1816–22 785	60 889	1.431
1	0.083	1592–17 953	46 652	1.474
1	0.167	1796–25 645	44 962	1.407
1	0.250	4203–38 065	3616	1.574

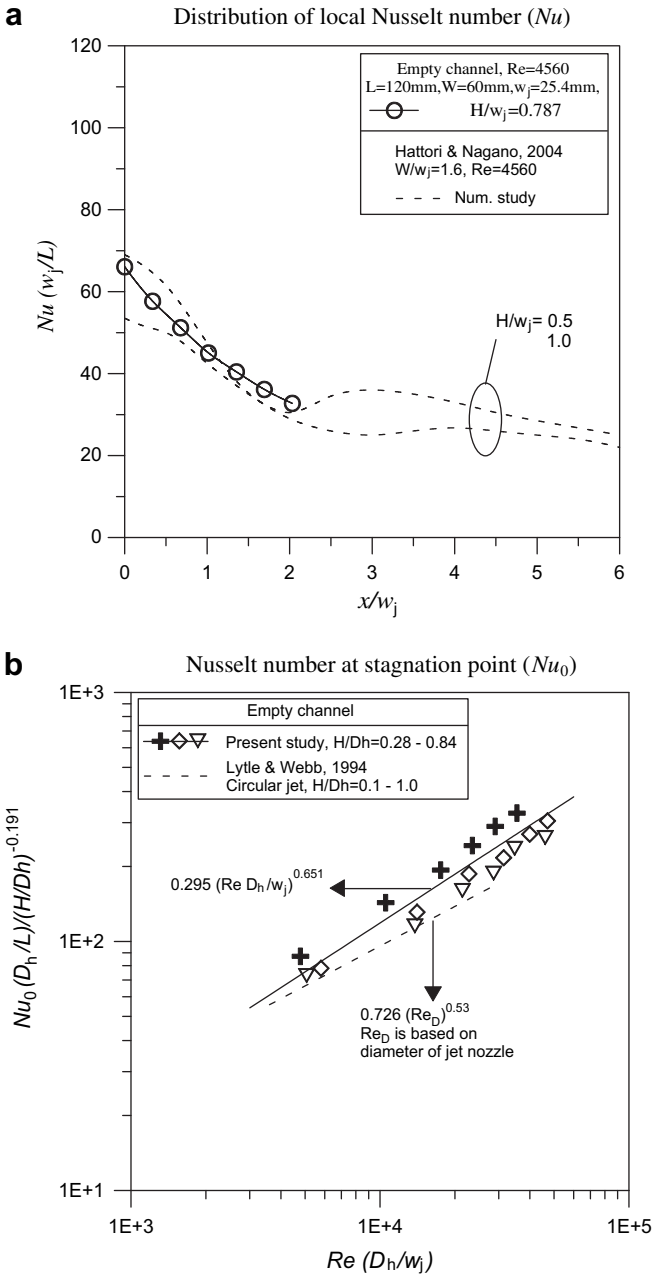

Fig. 5. Comparisons of Nu with others' data in jet cooling system without packed bed.

(d), the growing volume ratio of bead to packed bed will lead an increasingly stronger bypass effect at the near-wall region where the porosity is higher than the average porosity, neutralizing the increased pressure drop by decreasing H/L.

Fig. 4 illustrates the flow visualization of the fluid flow leaving the brass-beads packed bed. We used the smoke to represent the trace of flow. The smoke was obtained by burning the joss stick and collected in a box, and then blown into the test section by the compressor. The image capture system included a 60 mW He–Ne laser light-sheet illumination, a CCD camera and a computer. After passing through a 5 mm cylindrical quartz rod, the laser beam became a light sheet. As the light sheet illuminated the test section, the smoke reflected the laser light and the flow field in the test section could be easily observed. In order to obtain the optimal images, a fixed small flow flux ($Re = 858$) was employed. The images focus on the zone of the fluid flow leaving the brass-beads packed bed. It is found that, in the case of $w_j/L = 0.212$ as shown in Fig. 4(a), the leaving fluid flow generally became transverse flow along the channel axis due to the straightening effect of packed bed. Fig. 4(b) represents the flow characteristic of the case with $w_j/L = 1$. The photo shows that, the amount of fluid flow, through the upper corner of packed bed to leave for the transverse channel, was increased due to the minimal flow resistance of this path. This finding demonstrates the previous statement about the effect of w_j/L on pressure drop. The flow characteristic of big w_j/L also strongly influences the local heat transfer behavior, which is discussed in a later paragraph.

According to the experimental data, the relationship between dimensionless pressure drop ($C_f Re^2 (L/w_j)^2$) and Reynolds number (Re) was deducted below:

$$C_f Re^2 (L/w_j)^2 = m_1 Re^{n_1} \tag{6}$$

The values of m_1 and n_1 for various d, w_j/L and H/L were listed in Table 2, and the deviations between the predicted results by Eq. (6) and experimental data were within 2%.

3.2. Heat transfer

Due to the lack of experimental results for the impinging jet or the vertical oncoming flow onto the spherical packed bed, the jet cooling system without packed bed was employed to be the compared base. Fig. 5(a) indicates that, while the test channel was empty, the Nu distribution of present study reasonably agreed with the numerical result of Hattori and Nagano [27]. However, since the heated surface of present study was shorter, the second peak of Nu distribution could not be investigated. In addition, Fig. 5(b) compares the present data of Nusselt number at the stagnation point (i.e. $x/L = 0$) with the experimental result of Lytle and Webb [28]. The jet nozzle in the work of Lytle and Webb [28] was circular, while the present study was rectangular. The results of comparison verify the reliability of the present experiments.

Figs. 6 and 7 show the Nu distributions in the transverse flow direction (x-axis). Some typical cases were selected. The results

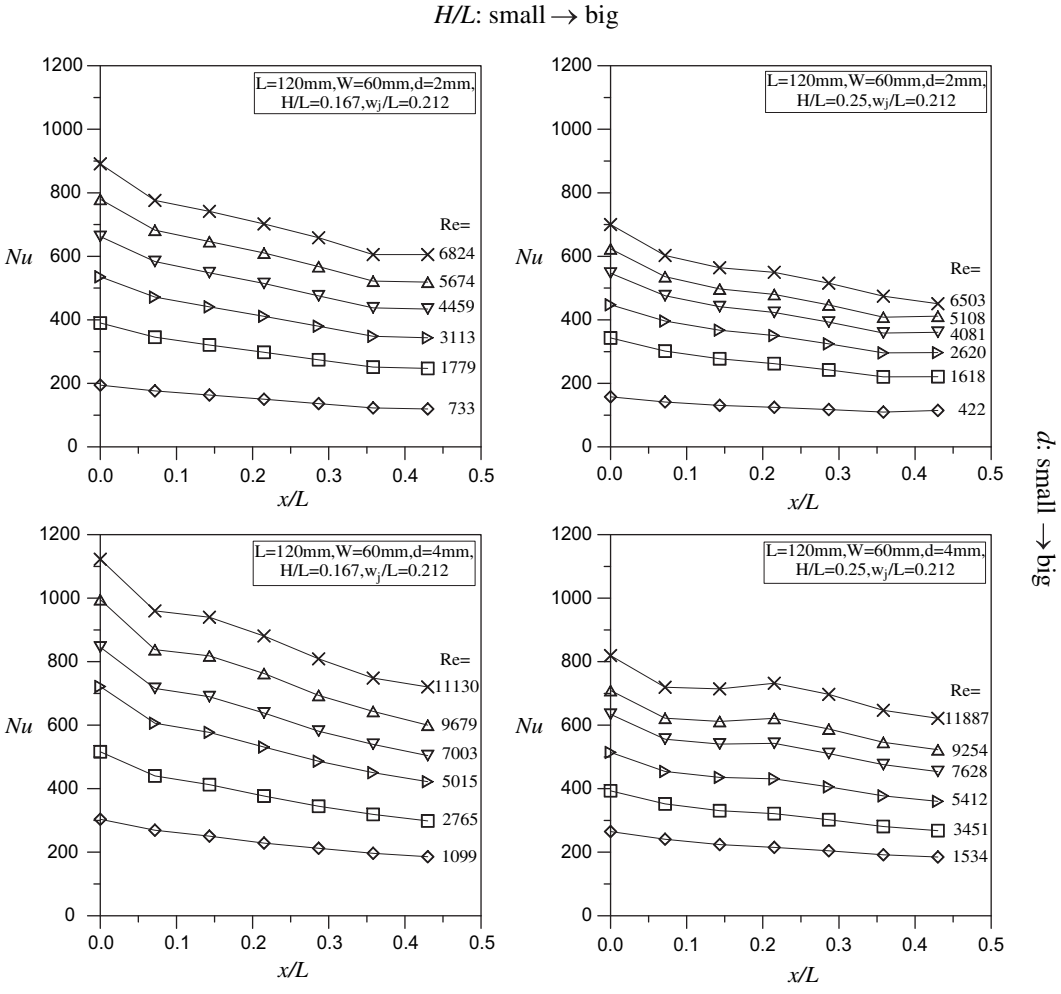

Fig. 6. Distributions of Nu along x-axis for the cases with $w_j/L = 0.212$ and various H/L, d and Re.

show that, in the cases of $w_j/L = 0.212$ with various H/L, d and Re, the Nu at the position under the flow entry (i.e. $x/L = 0$) was maximum and then decreased gradually along the x-axis. This Nu distribution corresponds to that of transverse flow in a porous channel Refs. [4,5], and also complies with the result of the impinging air jet onto aluminum foams reported by Jeng and Tzeng [23]. However, when the w_j/L became bigger, the Nu firstly decreased along the x-axis, and the minimal Nu happened about $x/L = 0.1$, then increased gradually until the exit of packed bed. The Nu at the exit of the brass-beads packed bed was even higher than that right under the flow entry ($x/L = 0$). This phenomenon of Nu distribution agrees with the finding of flow visualization as shown in Fig. 4. In the cases of bigger w_j/L, a lot of fluid flow through the upper corner of packed bed to leave for the transverse channel, strongly increasing the heat transfer at the lateral part of the packed bed.

Fig. 8 shows the average Nusselt number ($\overline{Nu}$) as a function of the Reynolds number (Re) for various w_j/L, d and H/L. The results indicate that the $\overline{Nu}$ increased with Re, conforming to the forced convective characteristics. Besides, the bigger w_j/L resulted in the smaller $\overline{Nu}$. This is because that, when the flow entry width (w_j) is closer to the packed-bed length (L), a great amount of airflow passes through and leaves from upper corners of brass-beads packed bed. The total extended heat-transfer area is not utilized effectively, leading to reduction of overall heat transfer. For the bead diameter (d), reduction of it slightly increased $\overline{Nu}$, which conforms to the finding of Jiang et al. [8] on brass-beads packed bed with transverse flow. As pointed out by Jiang et al. [8], there are many factors to influence the heat transfer of brass-beads packed bed, of which the transverse heat dispersion and the extended heat-transfer area play the important roles. The transverse heat dispersion refers to extra heat mixing behavior of fluids generated from the porous structure, which is expressed by the so-called transverse heat dispersion conductivity (k_d). The value of k_d is proportional to the fluid conductivity, flow velocity, Prandtl number and permeability of packed bed [11]. The permeability of packed bed increases with the bead diameter (d), so growing bead diameter (d) may strengthen the transverse heat dispersion conductivity (k_d) and then promote heat transfer, but also reduce the overall extended heat-transfer area against heat transfer. In general, when the stagnant conductivity of brass-beads packed bed is much bigger than the fluid conductivity (of this paper the stagnant conductivity is 0.398–0.578 W/m/K, the fluid conductivity about 0.027 W/m/K), the main heat transfer path is linked by heat conduction of brass-beads and then heat convection between beads and fluids. In such case, extended heat-transfer area plays an important role on overall heat transfer, so heat transfer will decline with the increase of bead diameter (d). But when the stagnant conductivity of brass-beads packed bed is almost the same magnitude with the fluid conductivity, the transverse heat dispersion effect cannot be ignored, and heat transfer may increase with the bead diameter [29,30]. Fig. 8 also depicts that the $\overline{Nu}$ increased

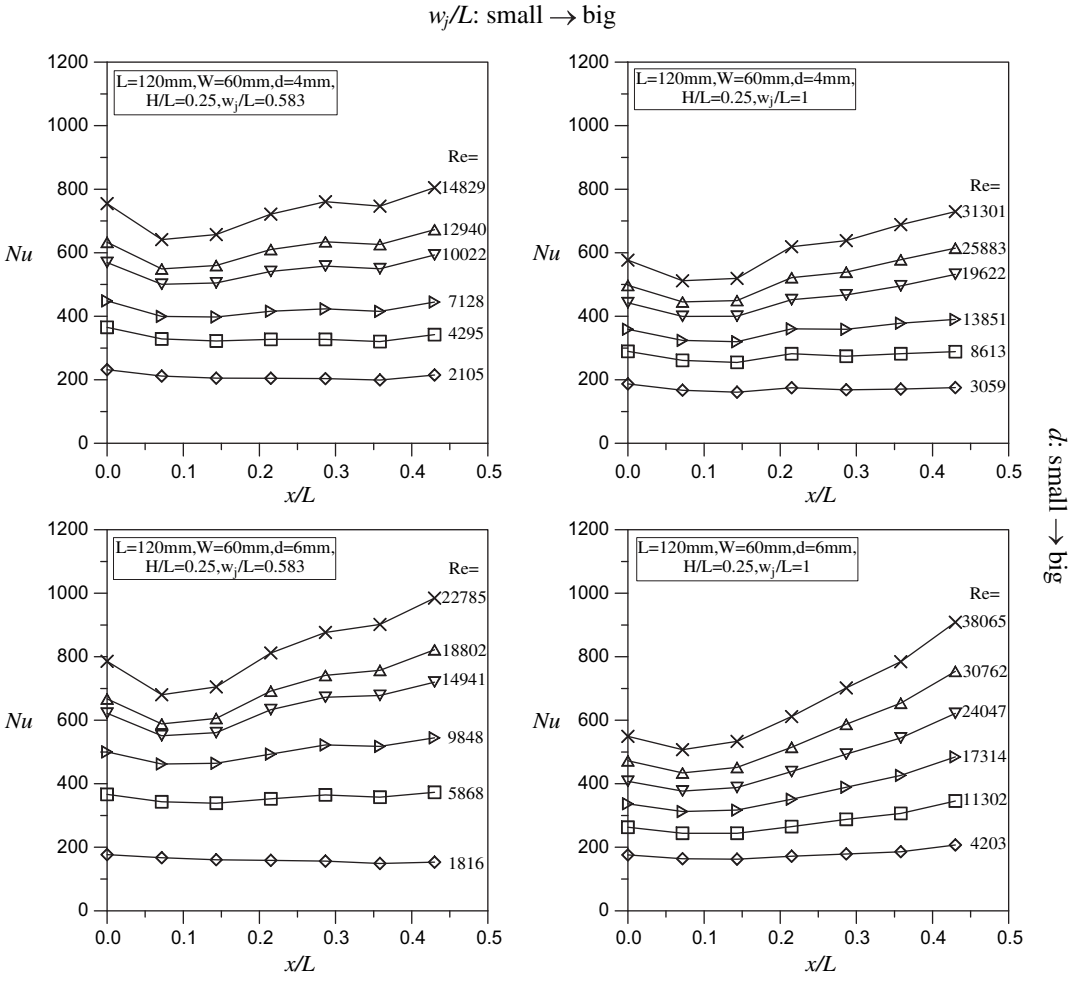

Fig. 7. Distributions of Nu along x-axis for the cases with $H/L = 0.25$ and various w_j/L, d and Re.

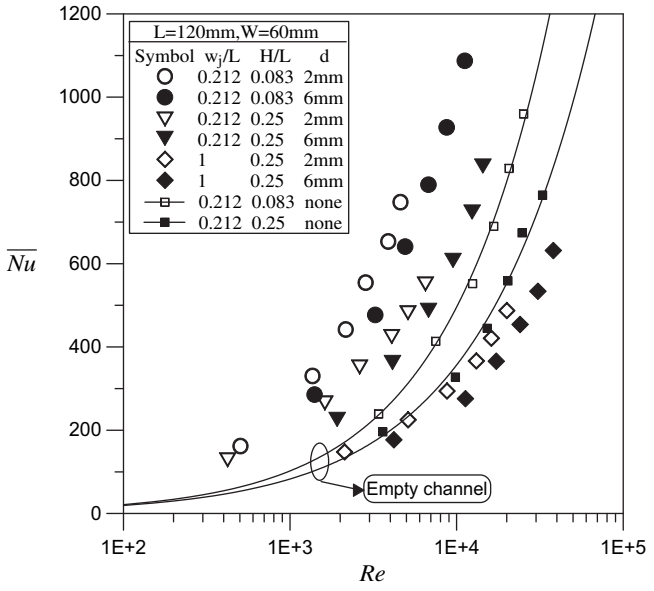

Fig. 8. $\overline{Nu}$ as a function of Re for various w_j/L, H/L and d.

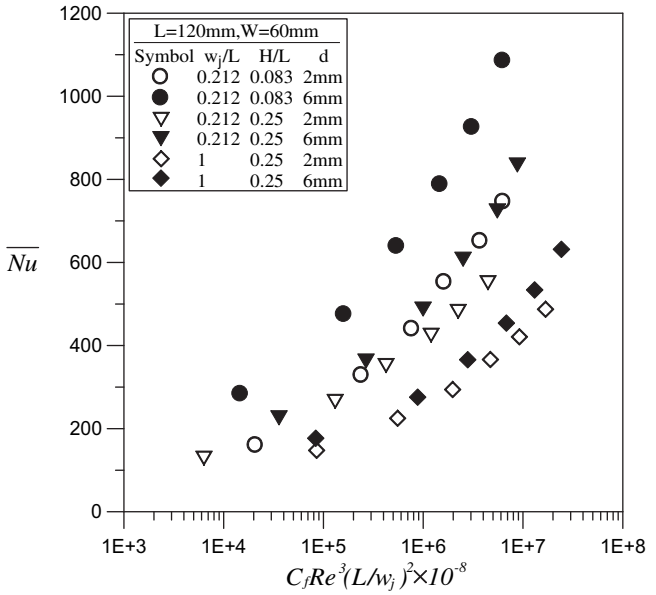

Fig. 9. $\overline{Nu}$ as a function of dimensionless pumping power for various w_j/L, H/L and d.

with decreasing the H/L. As we know, the packed bed of smaller H/L contained fewer numbers of brass beads, suggesting a smaller extended heat-transfer area to dissipate heat. However, the velocity of the transverse flow turned 90-degree from the flow entry increases with decreasing the H/L, enhancing the convective heat transfer between cooling fluid and brass-beads. Furthermore, the bigger fin efficiency at the packed bed of smaller H/L also promotes heat transfer. The above-mentioned hybrid effect of decreasing H/L led the result of increasing $\overline{Nu}$. Finally, the $\overline{Nu}$ of the system without packed bed was also plotted in Fig. 8. It can be found that the $\overline{Nu}$ of the system with packed bed was 2–3 times of that without packed bed.

Table 3
Coefficients of Eq. (7): $\overline{Nu} = m_2 Re^{n_2}$.

w_j/L	H/L	Re	m_2	n_2
$d = 2$ mm				
0.212	0.083	504–4603	2.262	0.688
0.212	0.167	733–6824	1.857	0.672
0.212	0.250	422–6503	5.277	0.530
0.583	0.083	648–6033	1.541	0.686
0.583	0.167	982–8149	1.842	0.646
0.583	0.250	1489–11 699	1.991	0.610
1	0.083	1668–13 622	0.248	0.765
1	0.167	2169–17 967	0.827	0.629
1	0.250	2123–20 035	2.581	0.525
$d = 4$ mm				
0.212	0.083	863–5878	1.551	0.744
0.212	0.167	1099–11 130	4.780	0.555
0.212	0.250	1534–11 887	3.018	0.580
0.583	0.083	1112–7916	1.529	0.702
0.583	0.167	1361–12 831	5.523	0.521
0.583	0.250	2105–14 829	2.022	0.607
1	0.083	2194–15 134	0.165	0.821
1	0.167	1632–25 832	1.744	0.552
1	0.250	3059–31 301	2.280	0.534
$d = 6$ mm				
0.212	0.083	1413–11 278	2.522	0.650
0.212	0.167	1541–13 383	3.403	0.580
0.212	0.250	1919–14 380	1.807	0.637
0.583	0.083	1585–11 880	2.272	0.615
0.583	0.167	2248–17 963	2.996	0.574
0.583	0.250	1816–22 785	1.469	0.630
1	0.083	1592–17 953	0.188	0.795
1	0.167	1796–25 645	1.944	0.557
1	0.250	4203–38 065	1.359	0.577

According to the experimental data, the relationship between $\overline{Nu}$ and Re was deducted below:

$$\overline{Nu} = m_2 Re^{n_2} \tag{7}$$

The values of m_2 and n_2 for various d, w_j/L and H/L were listed in Table 3, and the deviations between the predicted results by Eq. (7) and experimental data were within 2%.

3.3. Optimal configuration under same pumping power

It is found from previous results that, the bigger average Nusselt number ($\overline{Nu}$) and bigger pressure drop happened simultaneously. This work takes dimensionless pressure drop ($C_f Re^2 (L/w_j)^2$) multiplying Reynolds number (Re) as the parameter of dimensionless pumping power ($C_f Re^3 (L/w_j)^2$). The relationship between $\overline{Nu}$ and $C_f Re^3 (L/w_j)^2$ for various w_j/L, d and H/L are depicted respectively in Fig. 9. It is observed that, based on the same pumping power, the maximum $\overline{Nu}$ existed in the mode of the smallest w_j/L ($w_j/L = 0.212$), the smallest H/L ($H/L = 0.083$) and the biggest bead diameter ($d = 6$ mm), and the minimal $\overline{Nu}$ appeared in the mode of the biggest w_j/L ($w_j/L = 1$), the biggest H/L ($H/L = 0.25$) and the smallest bead diameter ($d = 2$ mm). The maximum $\overline{Nu}$ was around 3 times of the minimum $\overline{Nu}$ at the same pumping power in this study.

4. Conclusions

This work experimentally investigated the fluid flow and heat transfer characteristics of the vertical oncoming airflow onto the brass-beads packed bed. The brass-beads packed bed was fully filled in a rectangular channel. Variable parameters were the Reynolds number ($Re = 422$–38065), the ratio of packed-bed height to length ($H/L = 0.083$, 0.167, 0.25), the ratio of flow entry width to packed-bed length ($w_j/L = 0.212$, 0.583, 1) and the bead diameter ($d = 2$, 4, 6 mm). The influences of relevant parameters on the pressure drop and Nusselt number were discussed systemically.

The empirical equations of dimensionless pressure drop and average Nusselt number ($\overline{Nu}$) were also provided. Finally, it was suggested that the maximum $\overline{Nu}$, based on the same pumping power, existed in the mode of $w_j/L = 0.212$, $H/L = 0.083$ and $d = 6$ mm, and the minimal $\overline{Nu}$ appeared in the mode of $w_j/L = 1$, $H/L = 0.25$ and $d = 2$ mm. The maximum $\overline{Nu}$ was around 3 times of the minimum $\overline{Nu}$.

Acknowledgement

The authors would like to thank the National Science Council of the Republic of China for financially supporting this research under Contract No. NSC-97-2221-E-344-003 and NSC-97-2221-E-270-006.

Nomenclature

A	heated area (m^2)
C_f	friction factor, Eq. (2)
d	bead diameter (m)
D_h	hydraulic diameter of flow entry (m), $2w_jW/(w_j + W)$
H	packed bed height or test channel height (m)
h	heat transfer coefficient ($W/m^2/K$)
k	conductivity (W/m/K)
L	packed-bed length (m)
Nu	Nusselt number, Eq. (3)
Q_{in}	input heat (W)
Q_{loss}	heat loss (W)
Re	Reynolds number, Eq. (1)
T	temperature (°C)
U_e	average fluid velocity at the channel exit (m/s)
V_j	average fluid velocity at the flow entry (m/s)
W	packed-bed width or test channel width (m)
w_j	width of flow entry (m)
x	transverse flow coordinate (m)
ΔP	pressure difference through packed bed (Pa)
ΔS	spacing between adjacent thermocouples (m)

Greek symbols

ε	average porosity
μ	viscosity (kg/m/s)
ρ	density (kg/m^3)

Subscripts

d	transverse heat dispersion
f	fluid
j	flow entry
s	solid
w	heated wall
nw	near-wall region
∞	core region or ambient

Superscripts

—	mean value

References

[1] V.V. Calmidi, R.L. Mahajan, Forced convection in high porosity metal foams. J. Heat Transfer 122 (2000) 557–565.
[2] S.Y. Kim, B.H. Kang, J.H. Kim, Forced convection from aluminum foam materials in an asymmetrically heated channel. Int. J. Heat Mass Transfer 44 (2001) 1451–1454.
[3] K.C. Leong, L.W. Jin, Heat transfer of oscillating and steady flows in a channel filled with porous media. Int. Comm. Heat Mass Transfer 31 (2004) 63–72.
[4] G.J. Hwang, C.H. Chao, Heat transfer measurement and analysis for sintered porous channels. J. Heat Transfer 116 (1994) 456–464.
[5] G.J. Hwang, C.C. Wu, C.H. Chao, Investigation of non-Darcian forced convection in an asymmetrically heated sintered porous channel. J. Heat Transfer 117 (1995) 725–732.
[6] P.X. Jiang, M. Li, T.J. Lu, L. Yu, Z.P. Ren, Experimental research on convection heat transfer in sintered porous plate channels. Int. J. Heat Mass Transfer 47 (2004) 2085–2096.
[7] M.L. Hunt, C.L. Tien, Effects of thermal dispersion on forced convection in fibrous media. Int. J. Heat Mass Transfer 31 (1988) 301–309.
[8] P.X. Jiang, Z. Wang, Z.P. Ren, B.X. Wang, Experimental research of fluid flow and convection heat transfer in plate channels filled with glass or metallic particles. Exp. Thermal Fluid Sci. 20 (1999) 45–54.
[9] S. Polat, B. Huang, A.S. Mujumdar, W.J.M. Douglas, Numerical flow and heat transfer under impinging jets: a review. in: C.L. Tien, T.C. Chawia (Eds.), Annual Review of Numerical Fluid Mechanics and Heat Transfer, vol. 2. Hemisphere Publishing Corp., 1989, pp. 157–197.
[10] K. Jambunathan, E. Lai, M.A. Moss, B.L. Button, A review of heat transfer data for single circular jet impingement. Int. J. Heat Fluid Flow 13 (2) (1992) 106–115.
[11] W.S. Fu, H.C. Huang, Thermal performances of different shape porous blocks under an impinging jet. Int. J. Heat Mass Transfer 40 (10) (1997) 2261–2272.
[12] W.S. Fu, H.C. Huang, Effects of a random porosity model on heat transfer performance of porous media. Int. J. Heat Mass Transfer 42 (1999) 13–25.
[13] T.M. Jeng, S.C. Tzeng, Numerical study of confined slot jet impinging on porous metallic foam heat sink. Int. J. Heat Mass Transfer 48 (2005) 4685–4694.
[14] S.Y. Kim, J.M. Koo, A.V. Kuznetsov, Effect of anisotropy in permeability and effective thermal conductivity on thermal performance of an aluminum foam heat sink. Numer. Heat Transfer Part A 40 (2001) 21–36.
[15] S.Y. Kim, A.V. Kuznetsov, Optimization of pin-fin heat sinks using anisotropic local thermal nonequilibrium porous model in a jet impinging channel. Numer. Heat Transfer Part A 44 (2003) 771–787.
[16] H. Hadim, M. North, Forced convection in a sintered porous channel with inlet and outlet slots. Int. J. Thermal Sci. 44 (2005) 33–42.
[17] N.H. Saeid, A.A. Mohamad, Jet impingement cooling of a horizontal surface in a confined porous medium: mixed convection regime. Int. J. Heat Mass Transfer 49 (2006) 3906–3913.
[18] N.H. Saeid, Jet impingement interaction with cross flow in horizontal porous layer under thermal non-equilibrium conditions. Int. J. Heat Mass Transfer 50 (2007) 4265–4274.
[19] T.M. Jeng, S.C. Tzeng, Height effect on heat transfer characteristics of sintered porous blocks with a confined slot jet. Int. Comm. Heat Mass Transfer 35 (2008) 30–38.
[20] S.Y. Kim, M.H. Lee, K.S. Lee, Heat removal by aluminum-foam heat sinks in a multi-air jet impingement. IEEE Trans. Comp. Packag. Technol. 28 (2005) 142–148.
[21] W.H. Shih, W.C. Chiu, W.H. Hsieh, Height effect on heat-transfer characteristics of aluminum-foam heat sinks. ASME J. Heat Transfer 128 (2006) 530–537.
[22] S.C. Tzeng, T.M. Jeng, Convective heat transfer in porous channels with 90-deg turned flow. Int. J. Heat Mass Transfer 49 (2006) 1452–1461.
[23] T.M. Jeng, S.C. Tzeng, Experimental study of forced convection in metallic porous block subject to a confined slot jet. Int. J. Thermal Sci. 46 (2007) 1242–1250.
[24] E. Achenbach, Heat and flow characteristics of packed beds. Exp. Thermal Fluid Sci. 10 (1995) 17–27.
[25] S.J. Kline, F.A. Mcclintock, Describing uncertainties in single-sample experiments. Mech. Eng. (1953) 3–8.
[26] R.J. Moffat, Contributions to the theory of single-sample uncertainty analysis. ASME J. Fluids Eng. 104 (1986) 250–260.
[27] H. Hattori, Y. Nagano, Direct numerical simulation of turbulent heat transfer in plane impinging jet. Int. J. Heat Fluid Flow 25 (2004) 749–758.
[28] D. Lytle, B.W. Webb, Air jet impingement heat transfer at low nozzle-plate spacings. Int. J. Heat Mass Transfer 37 (1994) 1687–1697.
[29] P.X. Jiang, Z.P. Ren, B.X. Wang, Z. Wang, Forced convective heat transfer in a plate channel filled with solid particles. Int. J. Thermal Sci. 5 (1996) 43–53.
[30] P.X. Jiang, Z.P. Ren, B.X. Wang, Numerical simulation of forced convection heat transfer in porous plate channels using thermal equilibrium and non-thermal equilibrium models. Numer. Heat Transfer Part A 35 (1999) 99–113.